PCCP

Accepted Manuscript

ROYAL SOCIETY OF CHEMISTRY

www.rsc.org/pccp

Oxygen isotope exchange in $La_2NiO_{4\pm\delta}$

M. V. Ananyev[a, b1], E. S. Tropin[a], V. A. Eremin[a], A. S. Farlenkov[a], A.S. Smirnov[c], A. A. Kolchugin[a], N. M. Porotnikova[a], A. V. Khodimchuk[a,b], E. Kh. Kurumchin[a]

[a] Institute of High Temperature Electrochemistry, UB RAS, Laboratory of the Electrochemical Materials Science, Yekaterinburg 620137, Russia

[b] Ural Federal University named after the First President of Russia B.N. Yeltsin, Department of Chemical Engineering, Yekaterinburg 620990, Russia

[c] Institute of engineering science, Laboratory of Deformation Mechanics, UB RAS, Yekaterinburg 620049, Russia

Abstract

The oxygen surface exchange kinetics and diffusion have been studied by the isotope exchange method with gas phase equilibration using static circulation experimental rig at the temperature range of 600–800 °C and oxygen pressure range of 0.13–2.5 kPa. The novel model taking into account distributions of the dissociative adsorption and incorporation rates has been developed. The rates of the elementary stages have been calculated. The rate-determining stages for $La_2NiO_{4\pm\delta}$ polycrystalline specimen have been discussed. The diffusion activation energies calculated using the gas phase equilibration method (1.4 eV) differ significantly from those calculated using the isotope exchange depth profiling (0.5–0.8 eV), which was attributed to the influence of different oxygen diffusion pathways.

Keywords:

Lanthanum Nickelate, Oxygen Diffusion Coefficient, Oxygen Exchange Coefficient, Oxygen Isotope Exchange

Highlights:

- The oxygen surface exchange and diffusion coefficients for $La_2NiO_{4\pm\delta}$ are calculated.
- The model taking into account distributions of the dissociative adsorption and incorporation rates is proposed.
- A criterion of applicability for the developed model at every particular case is proposed.
- Rate-determining stages are considered
- The influence of the different oxygen diffusion pathways on the oxygen exchange kinetics is clarified.

[1]Corresponding author: tel. +7 343 362 3532, fax. +7 343 374 5992
Email address: m.ananyev@mail.ru

1. Introduction

Lanthanum nickelates attract the increasing attention of the scientific community due to high electronic and oxygen ionic conductivity and high catalytic activity in terms of oxygen reduction process. Previous studies have shown satisfactory thermal expansion properties along with relatively high oxygen diffusivity and fast surface exchange comparable with perovskite type materials based on cobaltites.[1–3] All mentioned above allows considering lanthanum nickelates as good cathode materials [4] in capacity of an alternative to the perovskite type mixed conducting oxides.

For clear understanding the oxygen electrode processes an information related to the interaction between gas phase and cathode material is required. Isotope exchange depth profiling by secondary ion mass-spectrometry method (IEDP SIMS) gives only the oxygen surface exchange coefficient k and cannot be used for clarification of the mechanism of the oxygen interaction with oxides. Only one work [5] is known related to the oxygen surface exchange mechanism description in $La_2NiO_{4\pm\delta}$ by means of pulsed isotope exchange technique. According to this study the dissociative adsorption is found to be the rate-determining stage. Figures 1, 2 and Tab. 1 summarize the literature data available concerning the temperature dependence of the oxygen surface exchange coefficient and the oxygen diffusion coefficient. A relatively large scatter in the data is observed because of the different synthesis approaches, surface preparation techniques, differences in microstructure, small deviations from cation composition etc.

The oxygen tracer diffusion in $La_2NiO_{4\pm\delta}$ was investigated in details by IEDP SIMS methods provide on polycrystalline ceramic [1], single crystals [7] and thin film specimens. [9] Strong anisotropy of diffusion was observed due to a layered structure of $La_2NiO_{4\pm\delta}$.[8] According to the experimental data the diffusion perpendicular to the (*ab*)-planes is 2–3 orders of magnitude slower than that along the (*ab*)-planes.[7–9]

The oxygen isotope exchange with the gas phase equilibration (GPE) on polycrystal samples provides an integral signal during the oxygen isotope exchange process including not only the surface exchange process, but also the contributions of diffusion processes: diffusion through differently oriented grains, grain boundary diffusion etc. Comparing GPE and IEDP results can help to understand the processes observed in different modifications of the oxygen isotope exchange method.

The aim of the present study is to examine the effect of the surface inhomogeneity and the anisotropy of diffusion on the oxygen exchange kinetics between the gas phase and $La_2NiO_{4\pm\delta}$.

2. Experimental

The $La_2NiO_{4\pm\delta}$ compounds were prepared using a two-step ceramic technology described elsewhere.[12]

The X-ray diffraction study was carried out on Rigaku D/MAX-2200VL/PC diffractometer in Cu K_α radiation. No peaks corresponding to impurity phases were observed (fig. 3). The obtained powder was pressed into slab specimens and sintered at 1450 ºC for 10 h. Having produced a dense material the specimens were polished with successive grades of diamond paste (ASM 7/5 NVM, grit size 5-7 μm and ASM 1/0 NOM, grit size 1 μm). The SEM images of the mechanically polished specimens shown in Fig. 4a. were observed by a scanning electron microscope TESCAN LYRA 3. The EDX analysis carried out on SEM Tescan Vega 2 (TESCAN, Czech Republic) equipped with the energy-dispersive spectrometer X-Act (Oxford Instruments, UK) revealed homogeneous distribution of La and Ni cations in the surface layer (fig. 4b and c). The electron backscatter diffraction (EBSD) experiments (fig. 5) were conducted using HKL Nordlys F+ spectrometer (Oxford Instruments, UK). The electron backscatter diffraction analysis allowed estimating the primary orientation of every grain for the considered surface area.

The isotope exchange was carried out in the static conditions with circulation. The experimental rig consisted of three main parts: the gas circuit connected to the quartz reaction chamber and the quadruple mass spectrometer with electron impact ionization. The scheme of the experimental rig is reported elsewhere.[13] Preliminary to the isotope exchange the sample underwent pre-treatment at 800 °C in oxygen. To prevent the oxygen gas diffusion obstacle the circulation pump was applied. Prior to the isotopic exchange samples were equilibrated with the gas phase consisting oxygen with a natural isotopic composition (0.2 at. % of ^{18}O) at the initial oxygen pressure and temperature. After the equilibrium was reached the reaction chamber was isolated from gas circuit and the gas circuit was filled with oxygen enriched by the ^{18}O isotope (83.5 at. % of ^{18}O). Then, the reaction chamber was again connected with the gas circuit and the isotopic exchange between the sample and the gas phase started. The composition of the phase was monitored during the oxygen exchange experiment by means of quadruple mass spectrometer Agilent 5973 N.

3. Theory

In the works of Muzykantov et al. [14] and Klier et al. [15] the three oxygen exchange types concept was developed. Depending on the number of oxygen atoms (or ions, ion-radicals) on the surface involved in one elementary interaction act (0, 1 or 2) all interactions between oxygen for the gas phase and solid oxide can be divided into three groups and every oxygen exchange type represents one of these groups:

$$^{18}O_2 + {}^{16}O_2 = 2{}^{16}O{}^{18}O \quad (1)$$

$$^{18}O_2 + {}^{16}O_s = {}^{16}O{}^{18}O + {}^{18}O_s \quad (2)$$

$$^{16}O{}^{18}O + {}^{16}O_s = {}^{16}O_2 + {}^{18}O_s \quad (3)$$

$$^{18}O_2 + 2{}^{16}O_s = {}^{16}O_2 + 2{}^{18}O_s \quad (4)$$

where O_s corresponds to the oxygen from the solid surface.

Reaction (1) corresponds to r_0 – oxygen exchange type associated with the direct interaction of the oxygen isotopes in the gas phase excluding the participation of the solid surface; reactions (2, 3) can be written as an example of r_1 – exchange type when 1 oxygen atom is replaced; and reaction (4) corresponds to r_2 – oxygen exchange type when 2 oxygen atoms are replaced. The three exchange types concept can be used for the tracer redistribution kinetics description in any system including the molecular oxygen in the gas phase and a solid.

More recently the two-step model was proposed by den Otter et al.[16] According to the model, a solid oxide surface is assumed to be homogeneous and two reactions take place. The first step is the dissociative adsorption (5), the second is incorporation stage (6).

$$O_2 + 2(\ )_a \overset{r_a}{=} 2O_a \quad (5)$$

$$O_a + (\ )_s \overset{r_i}{=} O_s + (\ )_a \quad (6)$$

where O_a corresponds to the oxygen adatom; O_s – is incorporated oxygen; $(\ )_a$ and $(\ )_s$ – are an adsorption site and oxygen vacancy on a solid surface, respectively; r_a – the adsorption reaction rate and r_i is the incorporation reaction rate.

In case of equilibrium between the gas phase and a solid oxide (when the oxygen pressure is constant) changing oxygen from the gas phase on the oxygen enriched by the ^{18}O-isotope, the kinetics of ^{16}O and ^{18}O isotopes redistribution can be studied using gas mass-spectrometry. Elementary acts (5) and (6) can be fixed for example for the incorporation stage (6) only after exchange between ^{18}O-adatom and incorporated ^{16}O isotopes or versa. Such that

for reactions (5) and (6) it is possible to write the equations of the isotope redistribution as follows:

$$O^{18}O + {}^{16}O_a \overset{r_a}{=} {}^{18}O_a + O^{16}O \quad (7)$$

$${}^{18}O_a + {}^{16}O_s \overset{r_i}{=} {}^{18}O_s + {}^{16}O_a \quad (8)$$

In the equation (7) the not labeled oxygen atom can correspond to either ^{16}O or ^{18}O isotope. The rates of three oxygen exchange types may be expressed via r_a and r_i:

$$r_0 = r_a(1-p)^2 = r\,\chi_0, \quad (9)$$

$$r_1 = 2p(1-p)r_a = r\,\chi_1, \quad (10)$$

$$r_2 = r_a p^2 = r\,\chi_2\ , \quad (11)$$

where p is revealed the probability of incorporation:

$$p = \frac{r_i}{r_a + r_i}, \quad (12)$$

χ_0, χ_1, χ_2 – contributions of three oxygen exchange types rates into overall oxygen exchange rate, r.

It is easy to conclude from (9–11) that for the two-step model the expression (13) holds:

$$\frac{2\sqrt{r_0 r_2}}{r_1} = 1 \quad (13)$$

However, in common case the oxide surface can be inhomogeneous. Consequently, as it was shown in [17], some kind of distribution of the oxygen heterogeneous exchange rate r_H and the oxygen overall exchange rate r is observed. In work [17], however, the reasons of r_H and r inhomogeneities are not discussed.

In our work the novel model for the explanation of the surface inhomogeneity possible reasons is proposed. For this reason one can consider inhomogeneity of the surface in connection with inequality of adsorption centers. Consequently, the adsorption rate and the incorporation rate have some distribution functions, $f(r_a)$ and $f(r_i)$, respectively. Obviously for homogeneous surfaces (where all adsorption centers are equal) these distributions are narrow such that it is possible to use only mean values for the adsorption or incorporation rates. In the extreme case of ideally homogeneous surface the distribution functions $f(r_a)$ and $f(r_i)$ are revealed by δ-functions and mean values of the dissociative adsorption and incorporation rates correspond to the r_a and r_i in the two-step model mentioned above.

In the case of inhomogeneous surface the oxygen exchange reaction mechanism can be written as a number of reactions. Thus, for each *k*-adsorption center we can write a couple of stages corresponding to the dissociative adsorption and incorporation with rates, r_{ak} and r_{ik} respectively:

$$\begin{cases} O^{18}O + {}^{16}O_{a1} \overset{r_{a1}}{=} {}^{18}O_{a1} + O^{16}O \\ {}^{18}O_{a1} + {}^{16}O_s \overset{r_{i1}}{=} {}^{18}O_s + {}^{16}O_{a1} \\ O^{18}O + {}^{16}O_{a2} \overset{r_{a2}}{=} {}^{18}O_{a2} + O^{16}O \\ {}^{18}O_{a2} + {}^{16}O_s \overset{r_{i2}}{=} {}^{18}O_s + {}^{16}O_{a2} \\ \cdots \\ {}^{18}O_{ak} + {}^{16}O_s \overset{r_{ak}}{=} {}^{18}O_{ak} + O^{16}O \\ {}^{18}O_{ak} + {}^{16}O_s \overset{r_{ik}}{=} {}^{18}O_s + {}^{16}O_{ak} \end{cases} \quad (14)$$

The equation system (14) can correspond to the following equation system:

$$\begin{cases} O_2 + (\ )_{a1} \overset{r_{a1}}{=} 2(O)_{a1} \\ (O)_{a1} + (\ )_s \overset{r_{i1}}{=} (O)_s + (\ )_{a1} \\ O_2 + (\ )_{a2} \overset{r_{a2}}{=} 2(O)_{a2} \\ (O)_{a2} + (\ )_s \overset{r_{i2}}{=} (O)_s + (\ )_{a2} \\ \cdots \\ O_2 + (\ )_{ak} \overset{r_{ak}}{=} 2(O)_{ak} \\ (O)_{ak} + (\ )_s \overset{r_{ik}}{=} (O)_s + (\ )_{ak} \end{cases} \quad (15)$$

In order to describe the isotope exchange kinetics it is necessary to write two kinetic equations related to ${}^{18}O$ fraction in the gas phase α and to deviation Z of ${}^{18}O_2$ concentration in the gas phase from its concentration $\alpha_2 = \alpha^2$ corresponding to the binomial isotope distribution.[18] For the equation system (14) the following kinetic equations are valid (constant multiplier is suppressed for simplicity, however, in general case, the r_a value is not dimensionless and have units):

$$\begin{cases} \dot{\alpha} = \sum_{k=1}^{K} r_{ak}(\alpha_{ak} - \alpha) \\ \dot{Z} = \sum_{k=1}^{K} r_{ak}(\alpha_{ak}^2 - \alpha_2) - 2\alpha\dot{\alpha} \end{cases}, \quad (16)$$

where K is total amount of adsorption centers.

At the equilibrium conditions according to the principle of the detailed equilibrium for each adsorption center the equation can be written as follows:

$$r_{ak}(\alpha_{ak} - \alpha) = r_{ik}(\alpha_s - \alpha_{ak}) \tag{17}$$

Deriving α_{ak} from (17) and substituting these values into (16) the following equation system is obtained:

$$\begin{cases} \dot{\alpha} = r_H(\alpha_s - \alpha) \\ \dot{Z} = -rZ + r_2(\alpha_s - \alpha)^2 \end{cases}, \tag{18}$$

where:

$$r_H = \sum_{k=1}^{K} g_k p_k r_{ak}\ , \tag{19}$$

$$r = \sum_{k=1}^{K} g_k r_{ak}\ , \tag{20}$$

$$r_2 = \sum_{k=1}^{K} g_k p_k^2 r_{ak}\ , \tag{21}$$

$$p_k = \frac{r_{ik}}{r_{ak} + r_{ik}}, \tag{22}$$

g_k – fraction of *k*-centers of adsorption on the surface, α_s – ^{18}O fraction at the oxide surface, p_k – the probability of incorporation for *k*-adatom.

Since

$$r_H = \tfrac{1}{2} r_1 + r_2, \tag{23}$$

$$r = r_0 + r_1 + r_2, \tag{24}$$

the rates of r_0 – and r_1 – oxygen exchange can be expressed as:

$$r_0 = \sum_{k=1}^{K} g_k r_{ak} - 2\sum_{k=1}^{K} g_k p_k r_{ak} + \sum_{k=1}^{K} g_k p_k^2 r_{ak}\ , \tag{25}$$

$$r_1 = 2\left(\sum_{k=1}^{K} g_k p_k r_{ak} - \sum_{k=1}^{K} g_k p_k^2 r_{ak}\right) \tag{26}$$

Taking (21), (25) and (26) into account it is easy to show that

$$\frac{2\sqrt{r_0 r_2}}{r_1} > 1 \tag{27}$$

Let us consider the influence of the distribution functions shapes of r_a and r_i on the $\frac{2\sqrt{r_0 r_2}}{r_1}$ parameter value, contributions of the three exchange types and the probability of

incorporation distribution, $f(p)$. For this estimation the r_a and r_i distribution functions were generated in MATLAB for three possible cases.

Case 1 corresponds to nearly homogeneous surface, and r_a and r_i have narrow Gaussian distribution (fig 6a). In this case the probability of incorporation also has narrow distribution similar to the Gaussian. If the distribution maximum $f(p)_{\max}$ exceeds 0.5, the dissociative adsorption is the rate-determining stage (fig. 6b.). If $f(p)_{\max}$ is less than 0.5 the incorporation is the rate-determining stage. The $\frac{2\sqrt{r_0 r_2}}{r_1}$ parameter value for case 1 is close to unity (see Tab.2).

Case 2 can correspond to the powder material consisting two fractions (relatively small and active particles and relatively large particles). In this case the existence of the bimodal distribution of the dissociative adsorption rate is possible (fig. 6c.). Two peaks of this distribution correspond to the more active and less active with respect to adsorption powder particles. Since both kinds of particles consist of the same compound one can conclude that the r_i distribution is more homogeneous and the incorporation rate distribution function is unimodal. In the considered case the probability of incorporation distribution function is unsymmetrical and $\frac{2\sqrt{r_0 r_2}}{r_1} > 1$ (see Tab.2).

Case 3 corresponds to two unimodal r_a and r_i distribution functions. Unlike the case 1 the half-width of the r_i distribution function is significantly higher comparing to the one of r_a (fig. 6e.). Case 3 can correspond to the homogeneous distribution of the adsorption centers on the surface and the inhomogeneous distribution of the oxygen sites associated with the incorporation stage. In the considered case the probability of incorporation distribution function is also unsymmetrical like in case 2. The probability of incorporation values vary from 0 to 1 with pronounced maximum at $p \approx 0.81$ and $\frac{2\sqrt{r_0 r_2}}{r_1} > 1$ (see Tab.2).

If $\frac{2\sqrt{r_0 r_2}}{r_1} = 1$ then the probability of incorporation distribution function is symmetrical which allows using the two-step model. Thus, ratio (11) may be used as a criterion of applicability of the two-step model in every particular case. If $\frac{2\sqrt{r_0 r_2}}{r_1} > 1$ then the probability of incorporation distribution function is unsymmetrical and the application of the two-step model

corresponds only to analysis of the mean values of r_a and r_i. Obviously, such analysis for unsymmetrical or polymodal distribution function is not always correct because a mode position or several positions of modes on a distribution do not fit the mean value of distribution.

For example in case 2 the incorporation rate distribution function has two modes with most probable values of $5 \cdot 10^{15}$ and 10^{16} whereas the mean value equals to $\approx 7.5 \cdot 10^{15}$ that corresponds to the minimum $f(r_a)$ between two maximums.

For application of the criterion (13) the calculation of the three exchange types rates is necessary. In the present work the rates of the three oxygen exchange types and the oxygen heterogeneous exchange rate were calculated for $La_2NiO_{4\pm\delta}$ using the model derived by Ezin at al [19] based on Klier's solution [20].

In conclusion it should be noted that the solution of the inverse problem (namely a determination of the adsorption and incorporation distribution functions shape using the parameter $\frac{2\sqrt{r_0 r_2}}{r_1}$ values) does not seem possible. However the parameter $\frac{2\sqrt{r_0 r_2}}{r_1}$ being higher than unity points at the surface inhomogeneity. The causes of such inhomogeneity should be considered at every particular case with involvement of additional surface investigation methods.

4. Results and discussion

4.1. Oxygen surface exchange kinetics

The experimental time dependencies of concentrations corresponding to $^{16}O_2$, $^{16}O^{18}O$ and $^{18}O_2$ (C_{32}, C_{34}, C_{36} respectively) at T = 800°C and p_{O2} = 5 Tor for $La_2NiO_{4\pm\delta}$ are presented in fig. 7. The experimental data treatment results for $La_2NiO_{4\pm\delta}$ by means of the three oxygen exchange types model and the two-step model are shown by lines in fig. 7a. and 7b., respectively. The sums of squared residuals (SSR) for the best fit data are 0.0039 and 0.0188 for three exchange types model and the two-step model, respectively. The difference between these results is statistically significant. Relatively large SSR for two-step model indicates that in the case of investigated $La_2NiO_{4\pm\delta}$ polycrystalline material the correlation (13) is not valid.

The temperature dependence of $\frac{2\sqrt{r_0 r_2}}{r_1}$ parameter is given in fig. 8. One can conclude that the ratio is more than unity (27) and increases with the temperature decreasing. Let us consider possible reasons of these deviations. As it was shown in the Theory section of this paper $\frac{2\sqrt{r_0 r_2}}{r_1}$ parameter exceeds unity in case of significant difference between the adsorption and incorporation distribution functions. On the assumption that the adsorption centers are bonded with Ni cations on the surface one can conclude that the r_a distribution appears unimodal given the homogeneous distribution of Ni cations at the surface confirmed by the EDX analysis (see fig.4c). In contrast, the r_i distribution can be associated with the oxygen sublattice and can be limited by the ^{16}O – oxygen diffusion to the surface and, hence, depends strongly on grain primary orientation since the anisotropy of the oxygen diffusion coefficient is observed. An EBSD map shown in fig. 5 illustrates a presence of grains with the primary orientation along the different crystallographic directions.

Our intention is that the model parameters for $La_2NiO_{4\pm\delta}$ are qualitatively most close to those in case 3, considered in the Theory section of this paper. The r_a and r_i distribution functions shapes for this case are illustrated in fig.6e. and 6f. Namely, the narrow unimodal r_a and broad r_i distribution functions are observed. Probably, the shape of the distribution functions for r_a and r_i depends on temperature: the lower temperature causes the broader distribution resulting in the increase of the $\frac{2\sqrt{r_0 r_2}}{r_1}$ parameter.

By means of the three oxygen exchange types model the values of the adsorption and incorporation rates can be calculated according to the following expressions:

$$r = r_a, \tag{28}$$

$$r_i = \frac{2rr_H}{r - r_H} \tag{29}$$

We assume that these values correspond to the mean values of r_a and r_i of the distribution functions $f(r_a)$ and $f(r_i)$. These values are plotted in fig. 9 at different p_{O2} in comparison with the data obtained in the work [5]. For each temperature both in our work and for data from [5] the incorporation rate is higher than the mean adsorption rate, moreover, the difference increases with the temperature decreasing. One can conclude that the dissociative adsorption is the rate-determining stage within the investigated temperature and oxygen pressure range. Furthermore, with the temperature increasing and the oxygen pressure decreasing the change of the rate-determining stage may become possible, such that at high temperatures and low oxygen pressures the oxygen surface exchange process can be limited by the incorporation. The oxygen pressure dependencies of the oxygen heterogeneous exchange rate, r_H, adsorption rate and incorporation rate appear to be fitted well by the power function. The power indices of r_H, r_a and r_i are reported in Tab. 3. The power index of r_H is governed by the power index of adsorption rate and is close to 0.5 which is in accordance with Langmuir's model of the dissociative adsorption.

The abovementioned considerations are based on the comparison of the mean values of r_a and r_i, however, the fact that ratio (13) is not equal to unity allows to conclude that the oxygen incorporation rate has a relatively broad distribution. The oxygen incorporation rate value can be 1–2 orders of magnitude higher comparing to the adsorption rate for the grains with the *(ab)*–crystallographic orientation (that corresponds to the dissociative adsorption being the rate-determining stage). In case of the grains with primary orientation along the *c*–axis incorporation rate is assumed to be very negligible. Consequently for such grains the oxygen surface exchange process can be limited by the incorporation.

4.2. Oxygen diffusion

The temperature dependencies of the oxygen diffusion coefficients obtained in works [1, 6–11] and our work are depicted in fig. 2.

The oxygen pressure dependence of the oxygen diffusion coefficient for different temperatures is depicted in fig. 10. One can observe that the oxygen diffusion coefficient hardly depends on the oxygen pressure which is in good agreement with the fact that the oxygen content in $La_2NiO_{4\pm\delta}$ is almost constant in the temperature range of 600–800 °C.[21]

The oxygen diffusion coefficients at 800 °C obtained in our work are in a good agreement with the literature data. With the temperature decreasing a significant difference between the oxygen diffusion coefficient obtained in the present work and the D values obtained by IEDP method is observed.

As it was already mentioned, according to the literature data [7–9] a significant anisotropy of the diffusion coefficient is observed along the different crystallographic directions. At higher temperatures the diffusion coefficient of $La_2NiO_{4\pm\delta}$ is close to the diffusion coefficient along the *ab* plane while at lower temperatures the diffusion coefficient obtained by GPE method for the lanthanum nickelate is close to the diffusion along the *c* axis [7]. The isotope exchange method with the gas phase equilibration allows obtaining some average (integral) diffusion coefficients including both the diffusion along the *ab* plane and the diffusion along the *c*-axis since the investigated sample $La_2NiO_{4\pm\delta}$ is polycrystalline. Besides the anisotropy of the diffusion the influence of the grain boundary diffusion should also be taken into consideration. Data obtained in the present work is insufficient to clearly divide the contributions to the oxygen diffusivity in polycrystalline $La_2NiO_{4\pm\delta}$.

5. Conclusions

The novel model considering the dissociative adsorption and incorporation distribution functions was proposed for describing the kinetics of the oxygen exchange between the gas phase and the solid oxide by comparing mean values of the dissociative adsorption and the incorporation rates. The proposed model was used for discussion of the results obtained in our work for $La_2NiO_{4\pm\delta}$.

The applicability criterion for the developed model at every particular case depending on the nature of the adsorption and incorporation rates distributions was suggested.

The carried out analysis allowed concluding that the distribution of the incorporation rate in $La_2NiO_{4\pm\delta}$ is relatively broad. The r_i value appear to be dependent on the grains primary orientation. For grains with the primary orientation along the *c*-axis, which have very low oxygen tracer diffusion coefficients and correspondingly negligible incorporation namely the incorporation is the rate-determining stage. The adsorption rates distribution was assumed to be uniform.

The influence of the different diffusion pathways on the oxygen exchange kinetics was clarified.

Acknowlegments

The facilities of the shared access center "Composition of Compounds" of IHTE UB RAS were used in this work. The authors thank B.D. Antonov for the XRD measurements. This work is financially supported by the RFBR projects № 14-03-00414 and 14-29-04009 and grants of the President of Russian Federation 2015-2017 (No. СП-1572.2015.1, СП-1663.2015.1).

References

1 S. Skinner, J. A. Kilner, *Solid State Ionics*, 2000, **135**, 709–712.

2 A. Berenov , A. Atkinson , J. Kilner , M. Ananyev , V. Eremin, N. Porotnikova , A. Farlenkov, E. Kurumchin, H.J.M. Bouwmeester, E. Bucher, W. Sitte, *Solid State Ionics*, 2014, **268**, 102–109.

3 J. B. Smith, T. Norby, *J. Electrochem. Soc.*, 2006, **153**, A233–A238.

4 K. Zhao, Y.-P. Wang, M. Chen, Q. Xu, B.-H. Kim, D.-P. Huang, *Int. J. Hydrogen Energy*, 2014, **39**, 7120–7130.

5 H. J. M. Bouwmeester, C. Song, J. Zhu, J. Yi, M. van Sint Annaland and B. A. Boukamp, *Phys. Chem. Chem. Phys.*, 2009, **11**, 9640–9643.

6 H. Zhao, F. Mauvy, C. Lalanne, J.-M. Bassat, S. Fourcade, J.-C. Grenier, *Solid State Ionics*, 2008, **179**, 2000–2005.

7 J. M. Bassat, P. Odier, A. Villesuzanne, C. Marin, M. Pouchard, *Solid State Ionics*, 2004, **167**, 341–347

8 N. Gauquelin, Ph D thesis, Aachen university, 2010, 226 p.

9 M. Burriel, G. Garcia, J. Santiso, J.A. Kilner, R.J. Chater, S.J. Skinner, *J. Mater. Chem.*, 2008, **18**, 416–422.

10 J.A. Kilner, C. K. M. Shaw, *Solid State Ionics*, 2002, **154-155**, 523–527.

11 V. A. Sadykov, N.F. Eremeev, V.V. Usoltsev, A.S. Bobin, G.M. Alikina, V.V. Pelipenko, E.M. Sadovskaya, V. S. Muzykantov, N.N. Bulgakov, N.F. Uvarov, *Russ. J. Electrochem.*, 2013, **49**, 645–651.

12 E.Yu. Pikalova, A.A. Kolchugin, N.M. Bogdanovich, D.I. Bronin, *Adv. Sci. Tech.*, 2014, **93**, 25–30.

13 E. K. Kurumchin, M.V. Ananyev, G.K. Vdovin, M.G. Surkova, *Russ. J. Electrochem.*, 2010, **46**, 205–209.

14 V. S. Muzykantov, *Kinet. Catal.*, 1965, **6**, 952–957.

15 K. Klier, J. Novakova, P. Jiru, *J. Catal.*, 1963, **2**, 479–484.

16 M. W. den Otter, B. A. Boukamp, H. J. M. Bouwmeester, *Solid State Ionics*, 2001, **139**, 89–94.

17 V. S. Muzykantov, G. I. Panov, *Kinet. Catal.*, 1972, **13**, 350–357.

18 V. S. Muzykantov, G. I. Panov, G. K. Boreskov, *Kinet. Catal.*, 1973, **14**, 948–951.

19 A.N. Ezin, E.Kh. Kurumchin, I.V. Murygin, V.I. Tsidilkovski, G.K. Vdovin, Solid *State Ionics*, 1998, **112**, 117–122.

20 K. Klier, E. Kucera, *J. Phys. Chem. Solids*, 1966, **27**, 1087–1095.

21 T. Nakamura, K. Yashiro, K. Sato, J. Mizusaki, *Solid State Ionics*, 2009, **180**, 368–376.

Titles of figures

Fig. 1 The temperature dependence of the oxygen surface exchange coefficient in $La_2NiO_{4\pm\delta}$ (numbers in the figure correspond to numbers at table 1).

Fig. 2 The temperature dependence of the oxygen tracer diffusion coefficient in $La_2NiO_{4\pm\delta}$ (numbers in the figure correspond to numbers at table 1).

Fig. 3 The XRD pattern of $La_2NiO_{4\pm\delta}$ powder and the unit cell of the $La_2NiO_{4\pm\delta}$ structure

Fig. 4 SEM-images of mechanically polished specimen of $La_2NiO_{4\pm\delta}$ for IE-GPE experiment:

a) secondary electron image; b) energy dispersive map for La; c) for Ni

Fig. 5 An EBSD map of the $La_2NiO_{4\pm\delta}$ surface: a) primary grains' crystallographic orientation map; Kikuchi lines on different grains without (b) and within refinement (c)

Fig. 6 Distribution functions of parameters for three cases (see text):

a, b – case 1; c, d – case 2; e, f – case 3; a, c, e – the adsorption and incorporation rates distribution functions; b, d, f – the probability of incorporation distribution functions for different cases

Fig. 7 The experimental time dependence of C_{32}, C_{34}, C_{36} concentrations in the gas phase fitted with a) three oxygen exchange types model; b) two-step model (T = 800°C, p_{O2} = 0.67 kPa)

Fig. 8 The temperature dependence of $\frac{2\sqrt{r_0 r_2}}{r_1}$ parameter, p_{O2} = 0.67 kPa.

Fig. 9 The oxygen pressure dependence of mean values of the oxygen heterogeneous exchange, dissociative adsorption and incorporation rates

Fig. 10 The oxygen pressure dependence of the oxygen diffusion coefficient for $La_2NiO_{4\pm\delta}$

Titles of tables

Tab. 1 Apparent activation energies for oxygen surface exchange and diffusion in $La_2NiO_{4\pm\delta}$

Tab. 2 Parameters of the developed model for three cases shown in fig. 6

Tab. 3 Power exponents of the heterogeneous exchange, dissociative adsorption and incorporation rates for $La_2NiO_{4\pm\delta}$

Fig. 1

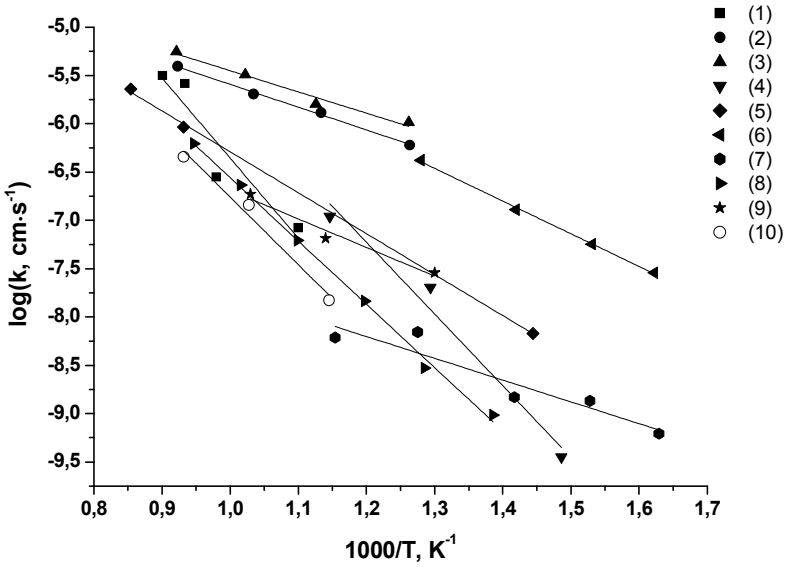

Fig. 2

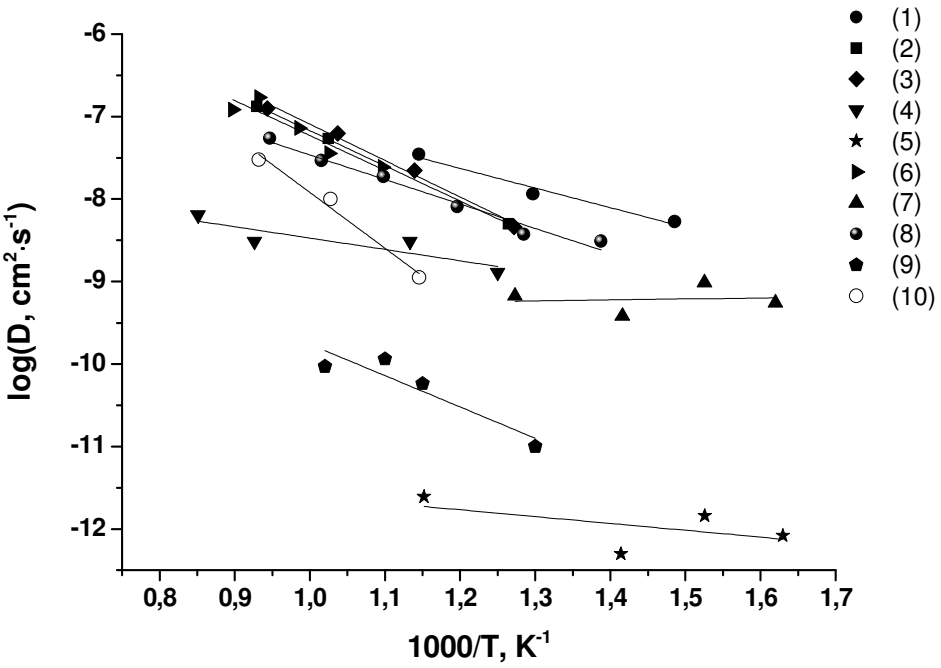

Fig. 3

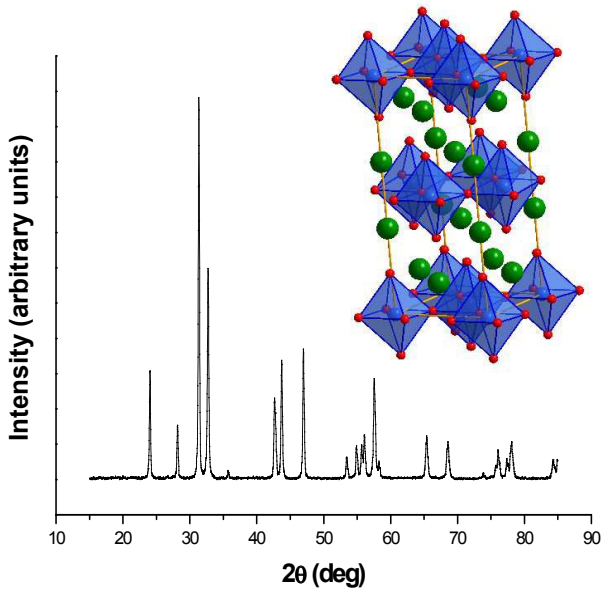

Fig. 4

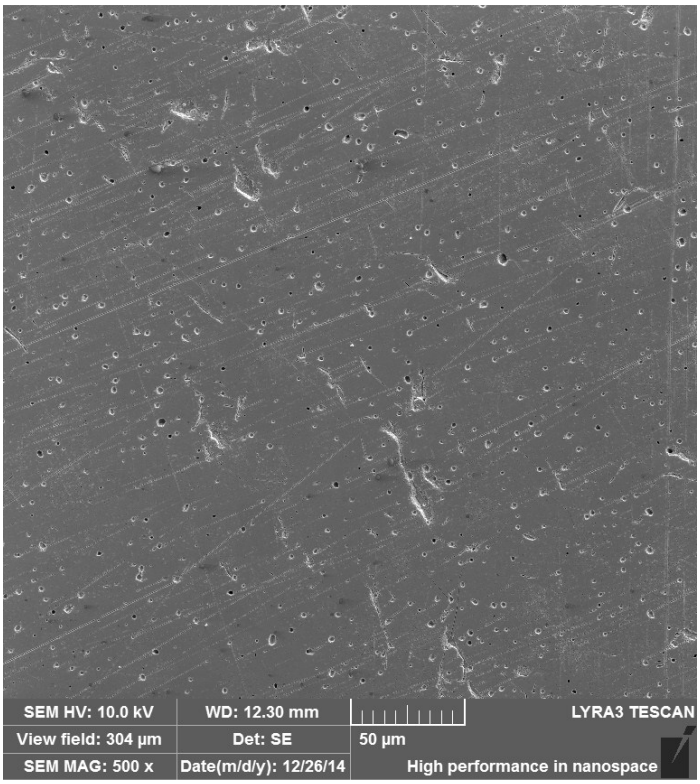

(a)

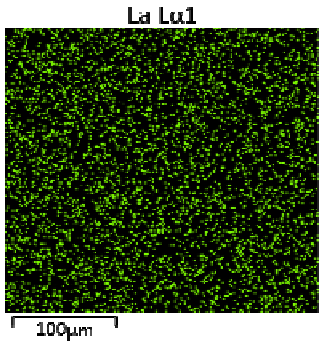

(b)

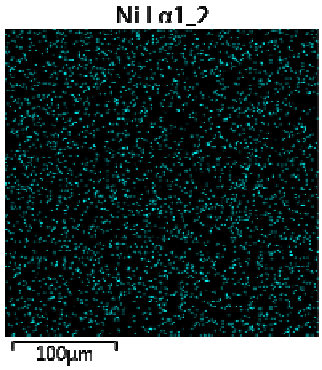

(c)

Fig. 5

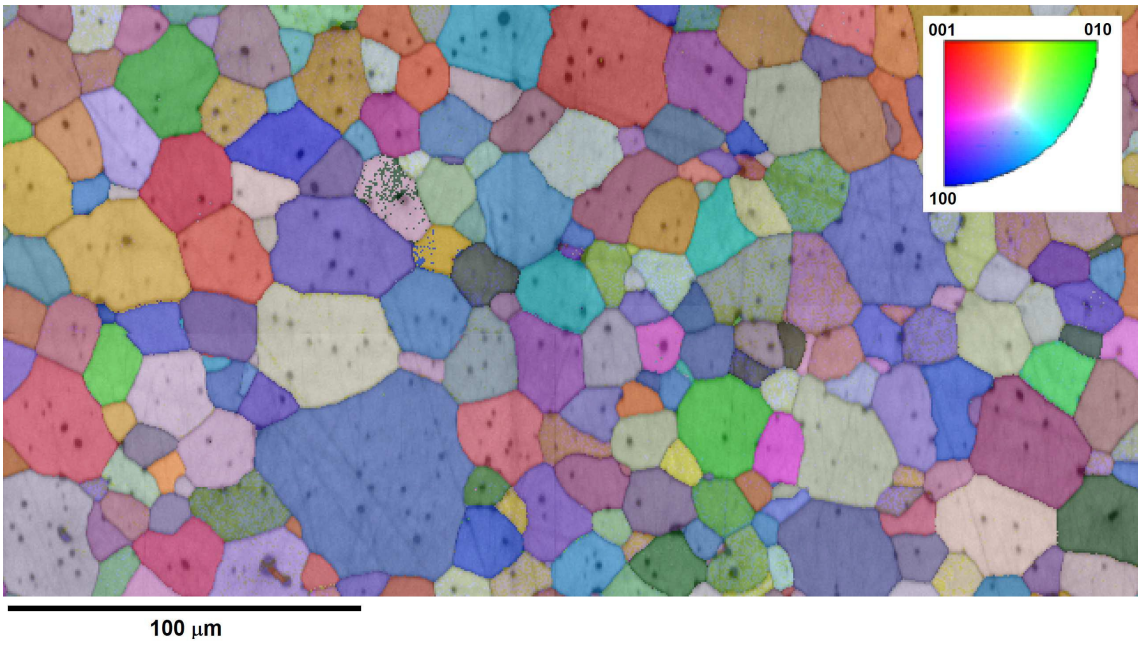

(a)

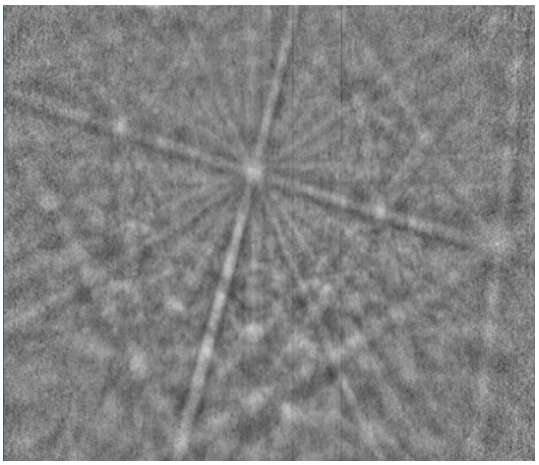

(b)

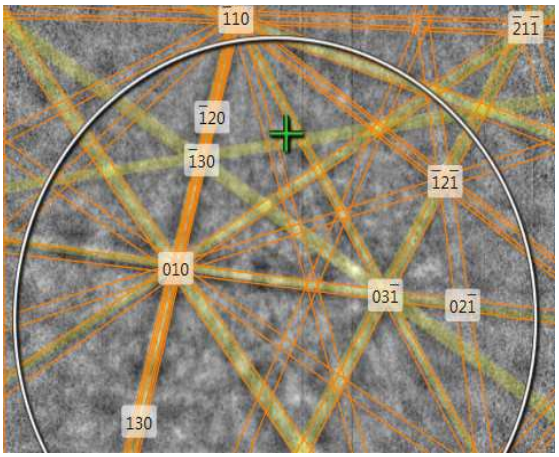

(c)

Fig. 6

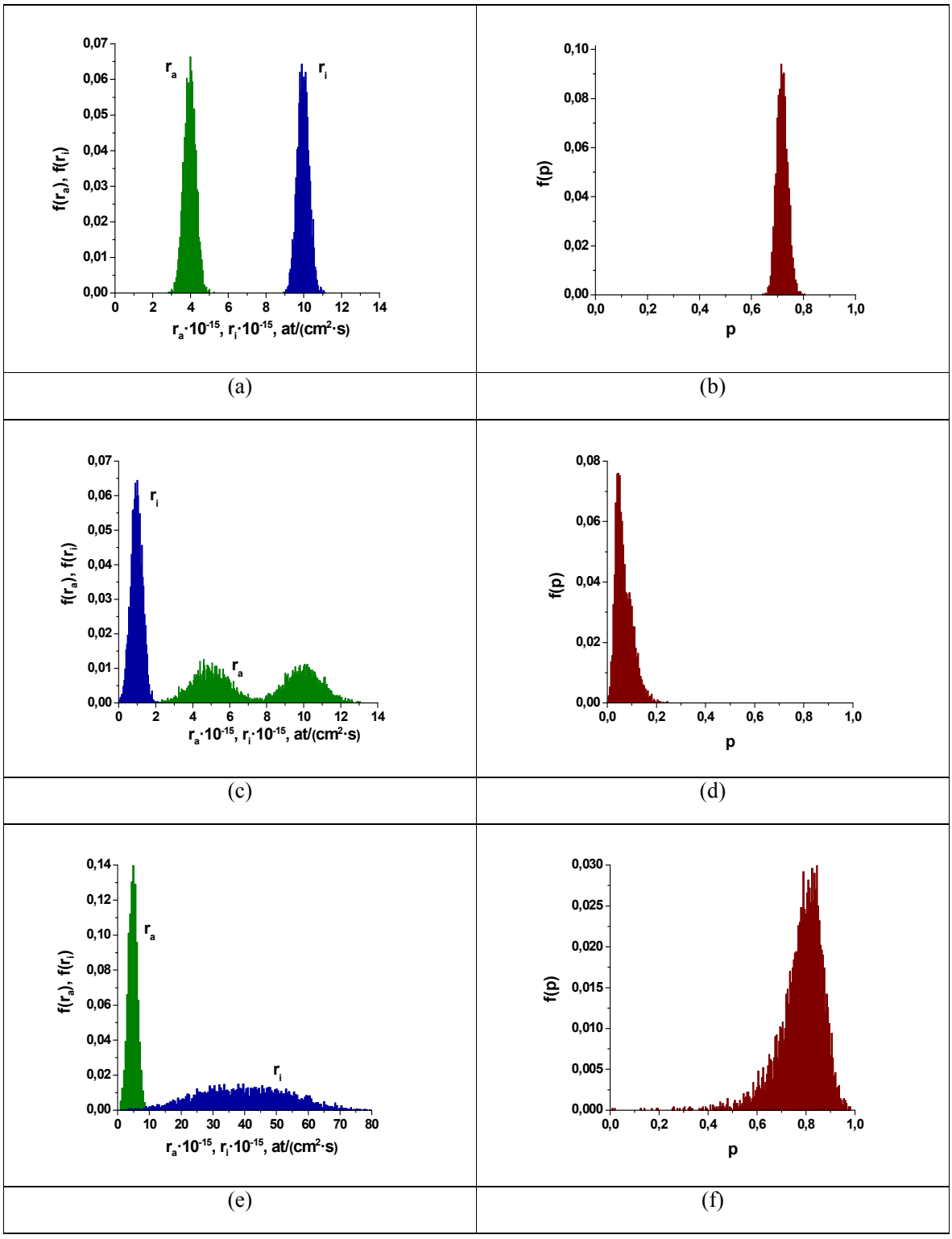

Fig. 7

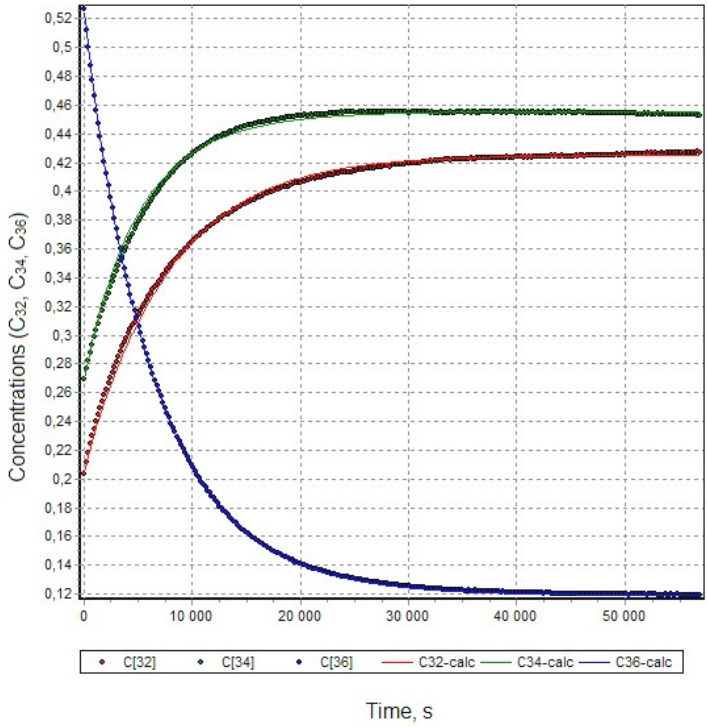

(a)

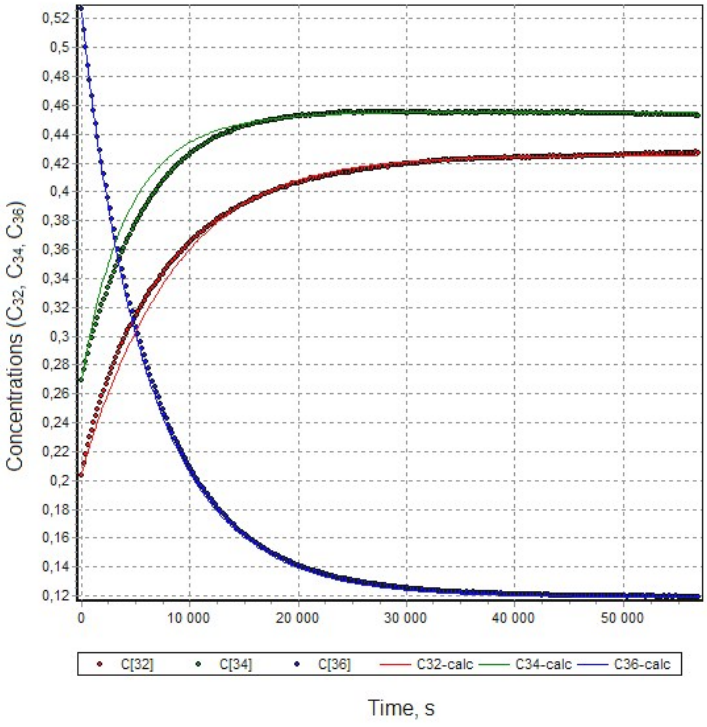

(b)

Fig. 8

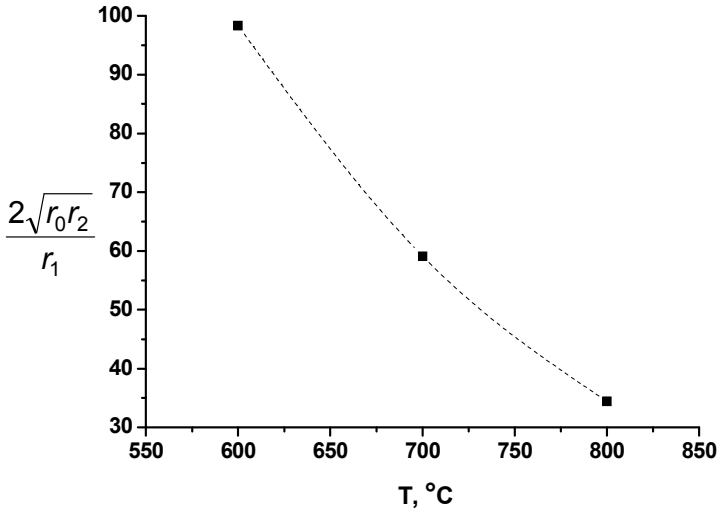

Fig. 9

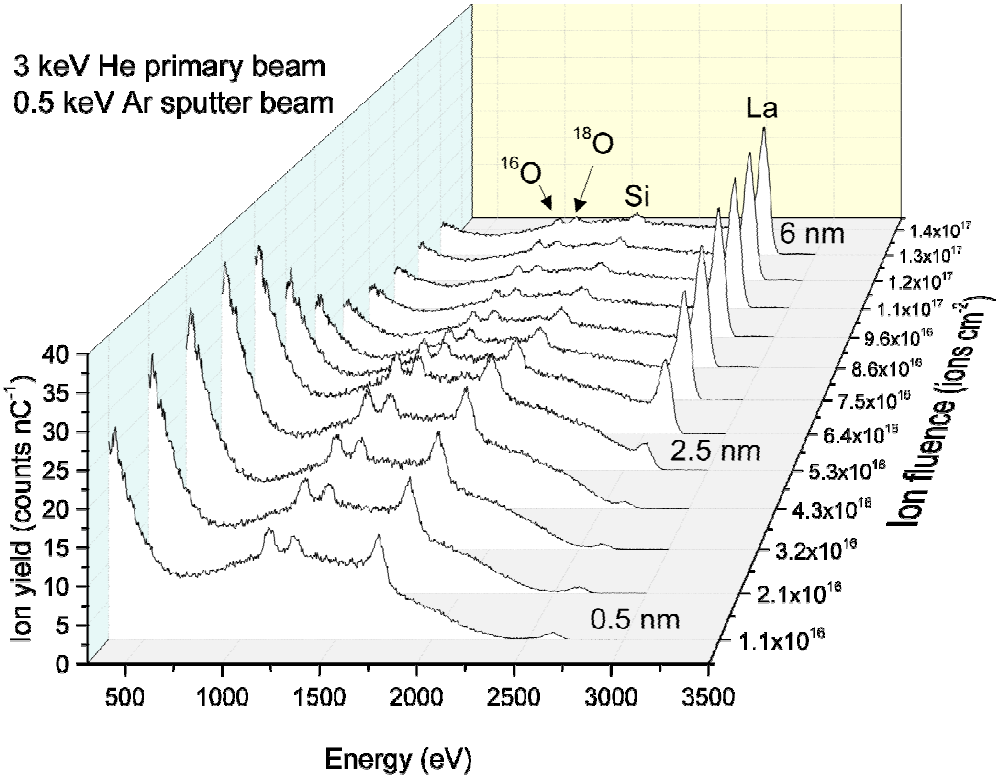

Fig. 10

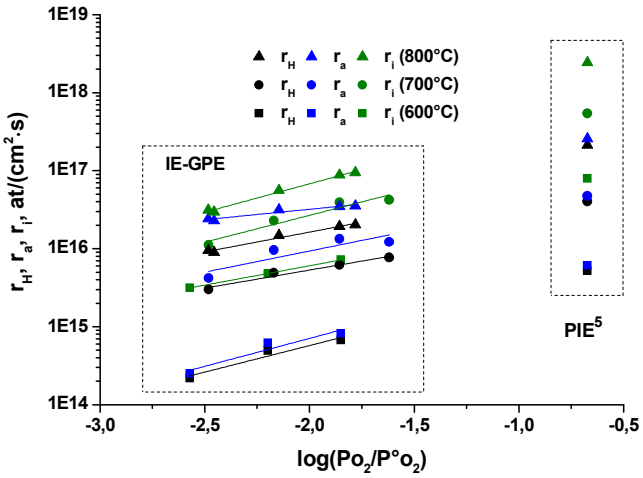

Fig.11

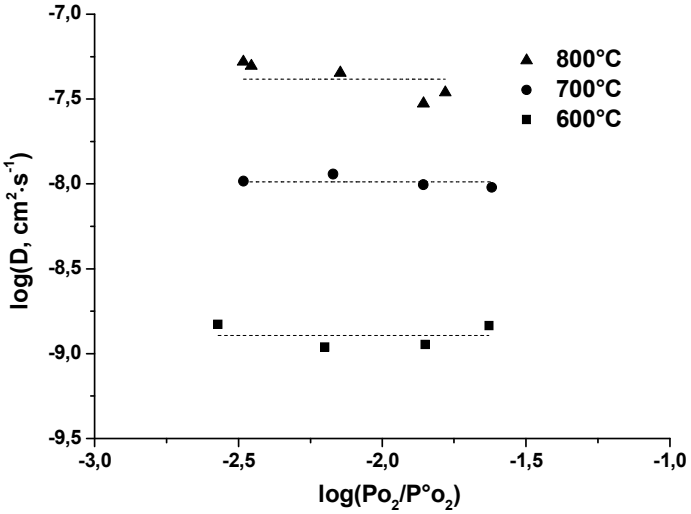

Table1. Apparent activation energies for oxygen surface exchange and diffusion in $La_2NiO_{4\pm\delta}$

Number of fig. 1–2	Po_2, kPa	T, °C	Apparent activation energy, eV		Method	Sample shape	Literature data
			Diffusion	Exchange			
1	101.3	640-842	0.85	1.61	IEDP/SIMS	Polycrystal	[1]
2	—	520-850	0.8	-	IEDP	Polycrystal	[6]
3	21.3	480-830	0.6-0.7	1.2-1.3	IEDP/SIMS	Single crystal oriented along *ab*-plane	[7]
4	100	400-600	0.47	1.48	SIMS line scan	Polycrystal	[8]
5	—	475-900	0.22	0.86	IEDP/SIMS	Single crystal oriented along *c*-axis	[7]
6	21.3	340-600	0.19	0.77	IEDP/SIMS	Thin film oriented along *ab*-plane	[9]
7	—	340-600	0.19	0.38	IEDP/SIMS	Thin film oriented along along *c*-axis	[9]
8	20	450-800	0.62	1.29	IEDP/SIMS	Polycrystal	[10]
9	21.3	750-950	0.75	0.59	IE-GPA	Polycrystal	[11]
10	1.33	600-800	1.41	1.38	IE-GPA	Polycrystal	Present work

Table 2. Parameters of the developed model for three cases shown in fig. 6.

Case	Parameters					
	r_H	r_a	$\frac{2\sqrt{r_0 r_2}}{r_1}$	χ_0	χ_1	χ_2
1	2.215±0.002	3.994±0.017	1.005±0.001	0.199±0.001	0.493±0.001	0.308±0.001
2	0.458±0,004	7.513±0,128	1.129±0,006	0.882±0.001	0.113±0.001	0.005±0.001
3	3.840±0.010	4.990±0.065	4.393±0.983	0.062±0.001	0.337±0.001	0.601±0.001

Table 3. Power exponents of the oxygen heterogeneous exchange, dissociative adsorption and incorporation rates for $La_2NiO_{4\pm\delta}$

T, °C	Power exponent		
	r_H	r_a	r_i
600	0.51(4)	0.51(5)	0.55(4)
700	0.46(5)	0.54(9)	0.68(8)
800	0.55(3)	0.44(5)	0.77(3)

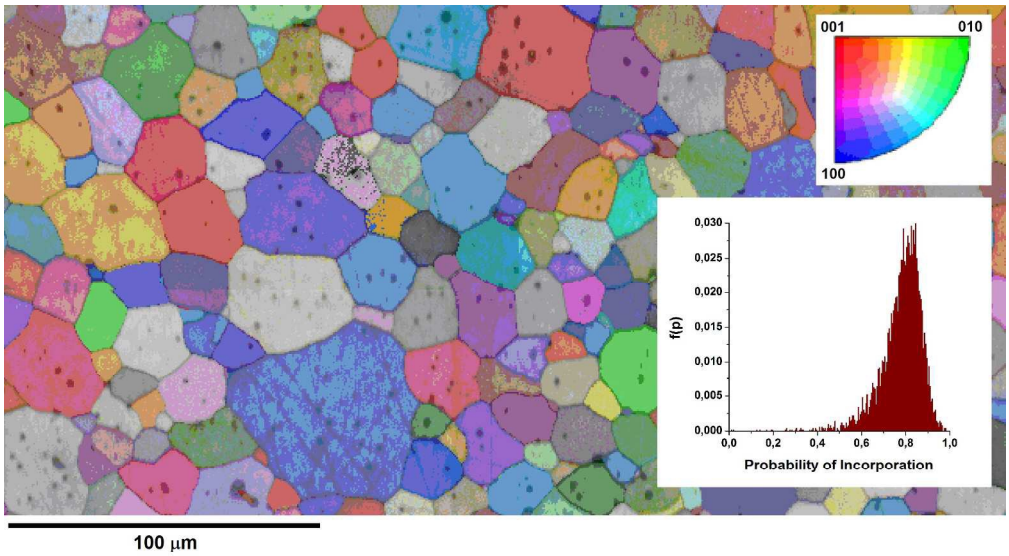

679x377mm (96 x 96 DPI)